
MAGPI SURVEY: Understanding dark matter halos of disk galaxies at $z \approx 0.3$

Project Report

By:

NIHARIKA SHRIVASTAVA
DEPARTMENT OF PHYSICS
INDIAN INSTITUTE OF SCIENCE EDUCATION AND RESEARCH, BHOPAL, INDIA

UNDER THE SUPERVISION OF:
DR. GAURI SHARMA
OBSERVATOIRE ASTRONOMIQUE DE STRASBOURG, FRANCE
DR. SHANTANU DESAI
INDIAN INSTITUTE OF TECHNOLOGY HYDERABAD

APRIL 2025

Abstract

This project aims to mass model the galaxy rotation curves using the MAGPI survey in the redshift range of 0.3 - 0.5 to understand the distribution of dark matter halos in galaxies. For initial stage of analysis, we create mock data using predefined baryonic and dark matter functions and then do the MCMC fitting to retrieve the parameters as to test whether our algorithm is performing accurately..

Table of Contents

Abstract	i
1 Introduction	1
1.1 Dark Matter	2
1.2 Probes for Dark Matter	2
1.2.1 Galaxy and galaxy clusters	3
2 Galaxy Kinematics and Dynamics	5
2.0.1 Galaxy Dynamics	5
2.1 Mass Models	7
2.1.1 Stellar component	7
2.1.2 Gas disc	8
2.1.3 Bulge component	9
2.1.4 DM halo component	10
2.2 Fitting Method	11
2.3 Galaxy Parameters and priors	12
3 Testing galaxy mock rotation curves	14
3.1 Corner and fitted Plots	16
3.2 Dark Matter Fraction	19
3.3 Analysis on multiple galaxies	21
3.3.1 Burkert halo mock data and Burkert halo fitting	21
3.3.2 NFW halo mock data and Burkert halo fitting	23
3.3.3 Burkert halo mock data and NFW halo fitting	25
3.3.4 NFW halo mock data and NFW halo fitting	27
3.3.5 Comparison with true values	29

TABLE OF CONTENTS

3.3.6	Dark Matter Fraction	30
3.3.7	Inference	30
4	MAGPI Observations	31
	Bibliography	32

Chapter 1

Introduction

One of the landmark achievements of the last decade of astronomical study is the establishment of a Standard model of cosmology. This theory gives us a simple consistent yet broad understanding of coherent explanations for the vast majority of complex cosmological phenomena. According to current observations of CMB and LSS (as depicted in fig. 1.1), the total energy budget of our universe consisting 69 % of dark energy, 26 % of dark matter(DM, hereafter) and 5 % of baryons(normal visible matter). The standard model of cosmology, the Λ CDM model, Λ representing the cosmological constant and CDM represents the cold dark matter, presents a good but not satisfactory explanation for all the observations (for details, (Peebles 1993)). There are still open questions regarding the existence and true nature of dark matter and dark energy. In this work, we assume this model and study the dark matter phenomenon and its interaction with baryonic matter in star-forming spiral disc galaxies.

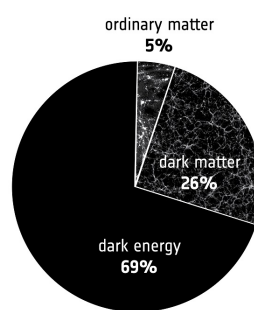


Figure 1.1: According to ESA's [Planck](#) mission, which obtained the most precise map of the cosmic microwave background, normal matter that makes up stars and galaxies contributes just about 5% of the Universe's mass/energy inventory. Dark matter, which is detected indirectly by its gravitational influence on nearby matter, occupies about 26%, while dark energy, a mysterious force thought to be responsible for accelerating the expansion of the Universe, accounts for the remaining 69% ([European Space Agency 2019](#))

1.1 Dark Matter

The concept of dark matter traces back to 1904 when Lord Kelvin suggested that the distribution and movement of stars in the Milky Way hinted at the presence of unseen, possibly extinct, dark stars (Knudsen 2005). Henri Poincaré later supported Kelvin's idea with observations in 1906, coining the term "dark matter" (Poincaré and Vergne 1911). Initial studies by Öpik (Öpik 2022) and Kapteyn (Kapteyn 1922) in the early 20th century found no evidence of dark matter, but James Jeans in 1922 (Jeans 1922) and Jan Oort in 1932 (Oort 1932) revised earlier methods, providing indications of a discrepancy between visible and total matter in the Milky Way. A significant breakthrough came in 1933 when Fritz Zwicky analyzed the Coma Cluster and found that galaxies moved much faster than expected based on visible mass alone. He concluded that a vast amount of unseen "dark" matter existed, a finding later confirmed by studies of the Virgo Cluster (Smith 1936).

The first direct evidence came from Babcock's 1939 Ph.D. thesis (Babcock 1939), where he noted that the rotational speed of the Andromeda galaxy did not match the expected Keplerian decline, suggesting a large amount of unseen mass. Subsequent confirmations by Oort, van de Hulst, Rubin (V. C. Rubin et al. 1978), Ford (Vera C. Rubin and Ford 1970), and others further cemented the idea of spherical distribution of dark matter, a "dark matter halo" surrounding galaxies to explain the observations. By the 1980s, studies by Albert Bosma (Bosma 1981) and others integrated these observations into cosmological models. Today, rather than questioning dark matter's existence, scientists seek to understand its true nature—whether it is a particle, fluid, or some other phenomenon.

1.2 Probes for Dark Matter

Unlike visible matter, dark matter does not interact with the electromagnetic force. This means it does not absorb, reflect or emit light, making it extremely hard to spot. In fact, we have been able to infer the existence of dark matter only from the gravitational effect it seems to have on visible matter. The major evidence for DM presence comes from interaction of visible and DM in galaxies and galaxy clusters. We can also indirectly observe DM using Cosmic Microwave Background(CMB) and gravitational lensing as well as other observation. In this work we focus on probing DM using galaxies as described below:

1.2.1 Galaxy and galaxy clusters

Dynamical studies of galaxies and galaxy clusters have been key to understanding dark matter([Zwicky 2009](#))[\(Paolo Salucci 2019\)](#)[\(Allen et al. 2011\)](#)[\(Vera C. Rubin and Ford 1970\)](#) and references therein). By analyzing the circular velocities of stars and gas through spectroscopic observations, scientists estimate the total mass enclosed in a given radius. In rotation-dominated systems like spiral and dwarf galaxies, this motion helps estimate mass, while in dispersion-dominated systems like galaxy clusters, velocity dispersion serves the same purpose. By using simple Newtonian physics we can write for galaxies:

$$M_{enc} = \frac{V_c^2(R)R}{G}$$

where M_{enc} is the total galactic mass within the radius R and G is the gravitational constant. The discrepancy between total mass M_{enc} (inferred from velocity) and luminous mass M_L (estimated from light) reveals the presence of dark matter. If visible mass followed light, these values would match i.e. $M_L = M_{enc}$, but observations show a significant excess of total mass—indicating a substantial, unseen “dark matter halo.”

To account for this mass discrepancy, the equation $M_{Halo} = M_{enc} - M_L$ is used. Studies focusing on rotation-dominated systems are more straightforward, while those on dispersion-dominated systems, like galaxy clusters, are more complex but still essential for understanding dark matter. In this work we focus on rotation dominated systems in local and intermediate redshift Universe ($z \approx 0.3$).

The standard Λ CDM model model, despite its success, faces several unresolved issues, particularly at small scales. These problems arise due to differences in the observations in galactic and extragalactic scales and the theory based simulations.

“Cusp-Core” problem This is a major unsolved problem refers to a discrepancy between the predicted and observed distribution of dark matter in the central regions of galaxies. This is particularly observable in low surface brightness disk and gas-rich dwarf galaxies due to their low baryonic density in inner regions as compared elliptical and massive spiral galaxies ([Blok 2009](#)). The rotation velocity associated with dark matter in the inner parts of disk galaxies is found to rise approximately linearly with radius. This solid-body behaviour can be interpreted as indicating the presence of a central core in the dark matter distribution, spanning a significant fraction of the optical disk. This behavior is modelled by Burkert Halo profile in our study ([Burkert 1995](#)). However, the results of numerical N-body simulations of dark matter halos

based on the collisionless cold dark matter (CDM) prescription did not show the observed core-like behaviour in their inner parts, but were better described by a steep power-law mass-density distribution, the so-called cusp. Simulations based on this model, such as those from the **Navarro-Frenk-White (NFW) profile** ([Navarro et al. 1996](#)), predict that dark matter halos should have a **cuspy** density profile, characterized by a steep, centrally concentrated distribution:

$$\rho(r) \propto \frac{1}{r^\gamma}$$

where $\gamma = 1$. However, observational studies of dwarf and LSB galaxies show that the dark matter density profiles in the central regions are more **core-like** than cuspy ([\(Palunas and Williams 2000\)](#)([P. Salucci and Burkert 2000](#)) ([de Blok et al. 2001](#))[\(Donato et al. 2004\)](#)[\(Simon et al. 2005\)](#)([P. Salucci, Lapi, et al. 2007](#))). These core profiles have a nearly constant central density, indicating a flat distribution of dark matter in the inner regions:

$$\rho(r) \propto \text{constant}$$

for small r . This mismatch is known as the **core-cusp problem**([Blok 2009](#)). Rotation curves of these galaxies, which trace the mass distribution, often show a flatter-than-expected rise near the center, contrasting the steep rise predicted by NFW profiles.

Chapter 2

Galaxy Kinematics and Dynamics

Galaxies are one of the most fascinating objects astronomers have observed, they come in various shapes and sizes, each having its own story of formation and evolution. The kinematic properties of a galaxy are studied under galaxy kinematics. Galaxy kinematics is a way to measure the motion of stars and gas that allows us to obtain fundamental information about the formation of galaxies and their current dynamical state. For example, kinematics derived from gas, which is collisional in nature, and stars, which are assumed to be collisionless (to a good approximation), allows us to disentangle various physical processes that occur on the galactic scale, such as: mass accretion and dynamical instabilities caused by supernovae (or AGN) feedbacks. The motion of the stars and gas also gives us the total amount of mass and its distribution within the galaxy as $V_c^2 = \frac{GM_{dyn}}{R}$, so does the shape of its potential under the Poisson's equation of gravitational potential ([Binney and Tremaine 2008](#)). That is, the galaxy dynamics derived from the observed kinematics is a portal to constrain the baryons and dark matter reside in the galactic potential wells.

2.0.1 Galaxy Dynamics

A galaxy, as a gravitationally bound system, has a gravitational potential that dictates its dynamics. This potential can be written as $\Phi(r) = GM(< r)/r^2$. The gravitational force for particles on circular orbits acts as a centripetal force, described by the equation $F = mV_c^2/r$. The radial change of the gravitational potential is related to the circular velocity, and can be expressed using Poisson's equation, which connects the gravitational potential to the system's mass density, including baryons and dark matter.

$$\frac{d\Phi}{dr} = \frac{V_c^2}{r}$$

$$\Delta\Phi = 4\pi G\rho$$

where ρ is the mass density of the system. Solving these two equations yield,

$$V_c^2 = \frac{4\pi G}{R} \int_0^R \rho(r)r^2 dx$$

This gives us the relation between circular velocity V_c and mass density ρ as a function from distance from the center of the galaxy. Using this we can obtain what we call the rotation curve of the galaxy. The rotation curve of a galaxy, which plots circular velocity against radius, serves as a key tool for studying mass distribution within the galaxy. For a typical disc-like galaxy the curve has contributions from various components—stellar disk, bulge, and halo. The rotation curve's flatness at large radii indicates the presence of dark matter, as the visible mass alone cannot account for the observed velocities.

To interpret the mass distribution, mass modeling techniques are employed. These methods vary based on the galaxy class and the quality of available data. The total circular velocity, $V_c(R)$, is a combination of contributions from baryons (stars and gas) and dark matter. It is given as a square root of sum of squares of individual components—specifically contributions from stellar disk, bulge, molecular and atomic gas, and the dark matter halo.

$$V_c^2(R) = V_D^2(R) + V_{bulge}^2(R) + V_{H2}^2(R) + V_{HI}^2(R) + V_{DM}^2(R) \quad (2.1)$$

where $V_D(R)$, $V_{bulge}(R)$, $V_{H2}(R)$, $V_{HI}(R)$ are the circular velocity profiles of the stellar disk, stellar bulge, molecular (H₂) and atomic (HI) gas disks, together providing the baryon's contribution to the circular velocity and $V_{DM}(R)$ gives the DM contribution. By analyzing these components, researchers can disentangle the contributions to the rotation curve and obtain a more accurate understanding of the galaxy's mass distribution, helping to distinguish between luminous and dark matter components.

In this work, we are using the rotation curves, derived from H α emission-line of galaxies. These rotation curves are modeled using 3D-Barolo (for details ([Sharma et al. 2022](#))). The resultant curves are corrected for beam-smearing ¹ and inclination ². We apply pressure gradient

¹Spectroscopic observations in the local Universe are accurate due to well-calibrated instruments and high resolution, allowing precise measurements of intrinsic circular velocity. However, for distant galaxies, limited angular resolution and beam spreading cause ‘beam smearing’, which blends nearby emission lines. This effect underestimates rotation velocity and overestimates velocity dispersion, especially in the inner regions, leading to a shallower rise in the rotation curve.

²Since we only observe the component of motion along our line of sight, the measured velocity is a projection

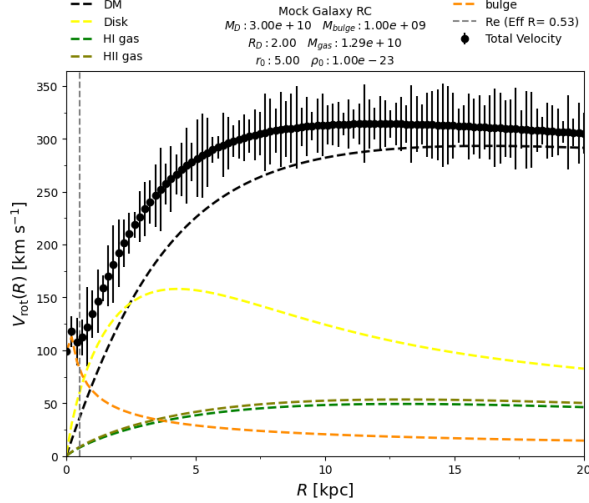


Figure 2.1: Mock rotation curve of galaxy having stellar disc length: 5 kpc, stellar mass: $3 \times 10^{10} M_{\odot}$, redshift : 0.3. The rotation curve is mass modelled using Burkert dark matter halo which has core radius: 5 kpc, and core density: $10^{-23} g cm^{-3}$.

correction³ on these rotation curves as done in ([Sharma 2021](#)), which we refer to as circular velocity curves. A mock rotation curve on predefined galactic parameters is shown in fig. 2.1

2.1 Mass Models

In this section we discuss the mass models of various components of rotation curve.

2.1.1 Stellar component

For the stellar and gaseous components of galaxies at high redshifts we use the exponential disk models as described in ([Freeman 1970](#)) for the local star-forming disks, dwarf-disks and low surface brightness galaxies([Persic et al. 1996](#)) ([Paolo et al. 2019](#)) ([Karuks and P. Salucci 2016](#)). The surface brightness can be written as:

$$\Sigma_-(R) \propto \frac{M}{R_{\text{scale}}} \exp\left(-\frac{R}{R_{\text{scale}}}\right), \quad (2.2)$$

of the true circular velocity, scaled by the sine of the inclination angle. Without correcting for this effect, the rotation velocity—and consequently, the dynamical mass—would be significantly underestimated

³In high-redshift star-forming galaxies, turbulence in the interstellar medium causes anisotropic and radially varying velocity dispersion, leading to a pressure gradient that supports the galaxy against gravity. This additional pressure support reduces the need for rotational support, resulting in slower disc rotation and declining rotation curves, even though dark matter continues to contribute fully to the gravitational potential.

where M and R_{scale} are the total mass and the scale length of the The various components of mass modeling are explained here.different components (stars, H₂ and HI), respectively. To denote the mass the mass of stellar disk we have used M_d whereas to find the total mass of stars we have $M_{star} = M_{bulge} + M_d$. Given the density distribution of the stars and the gas, their contribution to the circular velocity of the disk can be expressed as follows:

$$V_{disk}^2(R) = \frac{1}{2} \left(\frac{GM_d}{R_d} \right) (3.2x)^2 [I_0 K_0 - I_1 K_1], \quad (2.3)$$

where, $x = \frac{R}{R_{scale}}$ where $R_{scale} = 3.2 \times R_d$ and I_n and K_n are modified Bessel functions computed at 1.6x for stars ([Karukes and P. Salucci 2016](#))([Persic et al. 1996](#)).

2.1.2 Gas disc

To estimate the mass of molecular and atomic mass using stellar mass($M_{bulge} + M_d$), we first calculate the star formation rate of the star forming galaxies main sequence stars([Speagle et al. 2014](#)):

$$\log(SFR)(M_{star}, t) = (0.84 \pm 0.02 - 0.026 \pm 0.003 \times t) \log M_{star} - (6.51 \pm 0.24 - 0.11 \pm 0.03t) \quad (2.4)$$

where M_{star} is stellar mass and z is redshift, t is age of the Universe in giga years. We find atmoc and molecular gas mass using the scaling relations ([Tacconi et al. 2018](#)) ([Lagos et al. 2011](#)):

For molecular gas mass we have :

$$\mu_{\text{gas}} = A + B (\log_{10}(1+z) - F)^2 + C \log_{10} \left(\frac{\text{SFR}/M_{star}}{\text{MS_SFR}/M_{star}} \right) + D (\log_{10}(M_{star}) - 10.7)$$

using which we calculate:

$$M_{\text{HII}} = 10^{\mu_{\text{gas}}} \times M_{\text{star}} \quad (2.5)$$

with constants:

$$A = 0.06, \quad B = -3.33, \quad C = 0.51, \quad D = -0.41, \quad F = 0.65$$

For atomic gas mass:

$$\log_{10}(M_{\text{HI}}) = 0.32 \times \log_{10}\left(\frac{M_{\text{star}}}{10^{10}}\right) + 10.183 \quad (2.6)$$

for redshifts $0.4 < z < 1.04$ (Chowdhury et al. 2022). And then we use,

$$V_{\text{gas}}^2(R) = \frac{1}{2} \left(\frac{GM_{\text{gas}}}{R_{\text{gas}}} \right) (1.1x)^2 [I_0 K_0 - I_1 K_1], \quad (2.7)$$

for calculating V_{H2} and V_{HI} with modified bessel functions at 0.53x for gas. We have $R_{H2} = 1.5 \times R_d$ and $R_{HI} = 3 \times R_d$ (Karukes and P. Salucci 2016).

2.1.3 Bulge component

It has been well recognised that observed luminosity distribution for many elliptical and bulges is well described by:

$$\log_{10} \left[\frac{I(R)}{I(R_e)} \right] = -3.331 \left[\left(\frac{R}{R_e} \right)^{1/4} - 1 \right], \quad (2.8)$$

where R is the projected radius on the plane of the sky, R_e is the effective radius of the isophote enclosing half the light, and I is the surface brightness which is the famous de Vaucouleurs' $R^{1/4}$ law (de Vaucouleurs 1948). A density distribution which closely approximates this law has the form

$$\rho(r) = \frac{M}{2\pi r} \frac{1}{(r+a)^3} \quad (2.9)$$

where M is the total mass and a is a scale length. This then integrates into the mass form (Hernquist 1990):

$$M_r = M_b \frac{r^2}{(r+a)^2} \quad (2.10)$$

where effective half-light radius R_e is taken to be equal to a ($R_e = a$), is calculated using the spheroid size–mass relation, where different morphological types of galaxies are fitted with separate power-law relations. For S0 type of galaxies the R_e is described as (Hon et al. 2022):

$$\log(R_{e,\text{Sph}}/\text{kpc}) = 0.84 \log(M_b/M_\odot) - 8.81 \quad (2.11)$$

with this we find the velocity distribution of the bulge component:

$$V_{\text{bulge}}(r) = \frac{GM_r}{r} \quad (2.12)$$

where r is the distance from center.

2.1.4 DM halo component

In this work, we test two widely used DM halo models, namely the profiles of Burkert (Burkert 1995) and NFW (Navarro et al. 1996) as described in the cusp-core problem 1.2.1.

2.1.4.1 Burkert Halo (Cored halo)

Local spirals and low surface brightness galaxies suggest existence of central DM cores, that is $\rho_{inner} \propto const$. This observed DM-profile is well fitted by the Burkert (Burkert 1995) halo, which possesses a double power law in the DM-density, that is, at small radii $\rho \propto R^0$ and at larger radii $\rho \propto R^{-3}$. Such a DM-density distribution can be expressed as follows:

$$\rho(r) = \frac{\rho_0}{(1 + \frac{r}{r_0})(1 + \frac{r^2}{r_0^2})} \quad (2.13)$$

where ρ_0 and r_0 are the central DM core density and core radius, respectively. Assuming spherical symmetry, the mass profile of the Burkert DM halo can be expressed as follows:

$$M_{DM}^{Burk}(r) = 4\pi\rho_0 r_0^3 \left[\ln\left(1 + \frac{r}{r_0}\right) - \arctan\left(\frac{r}{r_0}\right) + 0.5 \ln\left(1 + \frac{r^2}{r_0^2}\right) \right]. \quad (2.14)$$

2.1.4.2 NFW Halo (Cuspy halo)

In the standard Λ CDM paradigm, the current cosmological simulations predict a cuspy DM distribution in the center, that is, $\rho_{inner} \propto R^{-1}$. This type of DM profile is well approximated by the NFW halo (Navarro et al. 1996), which is again a double power law; however, it has $\rho \propto R^{-1}$ at small radii and $\rho \propto R^{-3}$ at larger radii. Such a DM density distribution can be expressed as:

$$\rho(r) = \frac{\rho_s}{(\frac{r}{r_s})(1 + \frac{r}{r_s})^2} \quad (2.15)$$

where ρ_s and r_s are the characteristic density and scale radius of the DM distribution, respectively. Assuming spherical symmetry, the mass profile of the NFW DM halo is as follows:

$$M_{DM}^{NFW}(r) = 4\pi\rho_s r_s^3 \left[\ln\left(1 + \frac{r}{r_s}\right) - \frac{\frac{r}{r_s}}{1 + \frac{r}{r_s}} \right] \quad (2.16)$$

The circular velocity of the above DM profiles can be written as:

$$V_{DM}(r) = \frac{GM_{DM}}{r} (< r) \quad (2.17)$$

We can find the dark matter fraction within the radius r using

$$f_{DM} = \frac{M_{DM}}{M_{total}} = \frac{V_{DM}^2}{V_c^2} \quad (2.18)$$

2.2 Fitting Method

For mass modelling of our rotation curves we used principles of bayesian inference. Bayesian inference is a statistical approach used to estimate the parameters of a model by combining prior knowledge with observed data.

$$p(model(\theta)|Data) \propto p(Data|model(\theta)) \cdot p(model(\theta)) \quad (2.19)$$

where $model(\theta)$ represents a parameter (or a set of parameters) of interest, and $Data$ represents the observed data. Here, $p(model(\theta)|Data)$ is the posterior probability of $model(\theta)$ given the data, $p(Data|model(\theta))$ is the likelihood (the probability of the data given $model(\theta)$), and $p(model(\theta))$ is the prior (the a priori probability of $model(\theta)$). The symbol \propto denotes proportionality.

The process begins with defining a likelihood function, which measures the probability of observing the data given a set of model parameters. Specifically, the likelihood function compares the observed rotation velocities with the model-predicted velocities. A well-defined likelihood function ensures that the fit prioritizes models that closely match the data. Here we have used the function below (equation 2.20) as our likelihood function, a χ^2 test statistic on our observed kinematics $V_o(R)$ and modeled the kinematics $V_m(R)$ whereas σ represents the error in observed velocity.

$$\mathcal{L}_{\text{kin}} \equiv \prod_{k=1}^N \frac{1}{\sqrt{2\pi\sigma^2}} \exp \left[-\frac{1}{2} \left(\frac{V_o(R_k) - V_m(R_k)}{\sigma} \right)^2 \right]. \quad (2.20)$$

The posterior distribution is then obtained by multiplying the likelihood function with the prior distributions of the parameters. The priors represent any prior knowledge or assumptions about the model parameters, such as constraints from previous studies or theoretical limits. The posterior distribution thus encapsulates all available information about the model parameters, balancing the observed data with prior beliefs.

To estimate the posterior distribution, we use the Markov Chain Monte Carlo (MCMC) method, specifically the “emcee” Python package ([Foreman-Mackey et al. 2013](#)). MCMC is a computational technique that generates samples from the posterior distribution by constructing a Markov chain that explores the parameter space. In the study, 100 MCMC walkers are run for 10,000 steps, resulting in 10^6 samples. The initial 500 of these samples serves as the “burn-in” period to allow the chains to converge, reducing the influence of initial guesses.

In the next section approach’s reliability is validated by applying it to synthetic rotation curves generated from known model parameters. Successful recovery of these input parameters within 1σ uncertainties demonstrates the method’s robustness. Overall, Bayesian inference combined with MCMC sampling provides a powerful and reliable method to disentangle baryonic and dark matter components in galaxy mass modeling.

2.3 Galaxy Parameters and priors

In the next chapter we perform a mock analysis for optimal performance of our algorithm and present fitting results. We have used the the following parameters for mass modeling of galaxies:

1. Stellar disk mass (M_d)
2. Stellar disk radius (R_d)
3. Atomic gas mass (M_{HI})
4. Molecular gas mass (M_{H2})
5. Bulge mass (M_b)
6. DM core/cusp radius (r_0)
7. DM core density (ρ_0)

We have set the following priors for our MCMC analysis.

These are the priors for all the parameters for mock analysis.TV = True value

Parameter Range	Prior: Central Value, Sigma
$8 < \log(M_d) < 12(M_\odot)$	Gaussian Prior: $TV, 0.05 \times TV$
$-1.7 < \log(R_d) < 1.7(kpc)$	Gaussian Prior: $TV, 0.05 \times TV$
$7 < \log(M_{HI}) < 11(M_\odot)$	Gaussian Prior: $TV, 0.05 \times TV$
$7 < \log(M_{H2}) < 11(M_\odot)$	Gaussian Prior: $TV, 0.05 \times TV$
$5 < \log(M_b) < 11.5(M_\odot)$	Gaussian Prior: $TV, 0.1 \times TV$
$-2 < r_0 < 2(kpc)$	Flat Prior
$-26 < \rho_0 < -18(g/cm^3)$	Flat Prior

Table 2.1: Mass modeling Parameter Ranges and Priors details. Here, we have stellar disk mass (M_d), Stellar disk radius (R_d), Atomic gas mass (M_{HI}), Molecular gas mass (M_{H2}), Bulge mass (M_b), DM core/cusp radius (r_0) and DM core density (ρ_0)

Chapter 3

Testing galaxy mock rotation curves

This is initial training part of our study to test our algorithm to obtain galactic parameters. Firstly we generate mock data using some predefined parameters on mass models as defined previously and then feed the mock data into our MCMC algorithm to retrieve the parameters. The values of these parameters is described in table 3.1

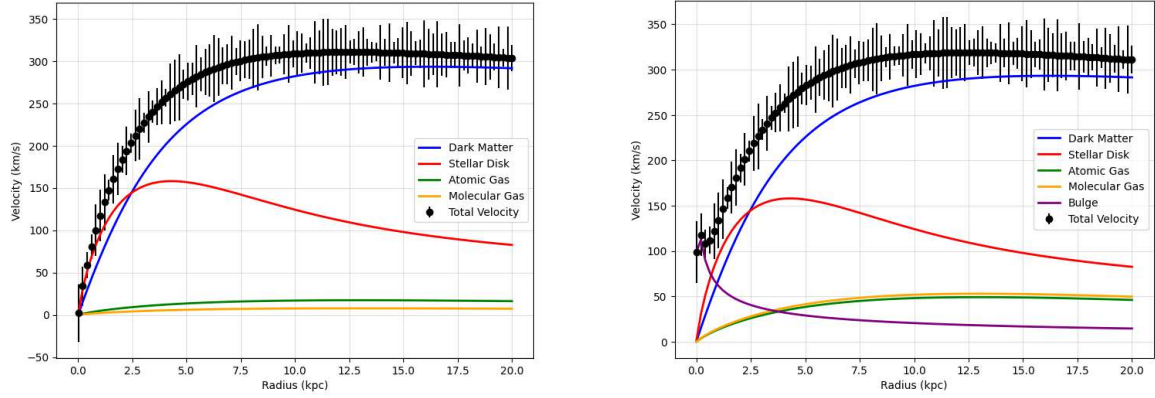
Galactic Parameters	Values
r_0	5 Kpc
ρ_0	$1 \times 10^{-23} \text{ g/cm}^3$
R_d	2 Kpc
M_d	$3 \times 10^{10} M_\odot$
M_{bulge}	$10^9 M_\odot$
M_{HI}	$10^9 M_\odot$
M_{H_2}	$10^8 M_\odot$

Table 3.1: Predefined Galactic Parameters and their true values. Here, we have stellar disk mass (M_d), Stellar disk radius (R_d), Atomic gas mass (M_{HI}), Molecular gas mass (M_{H_2}), Bulge mass (M_b), DM core/cusp radius (r_0) and DM core density (ρ_0)

We have taken $R_{\text{gaseous disk}} = 3 \times R_d$ and $R_{\text{eff}} = 1.69 \times R_d$. The following data has been generated for $R = 0.01$ Kpc to 20 Kpc with 100 equally spaced steps and random errors.

Here we have generated 4 different variations of mock data which are as follows figures (3.1 & 3.2):

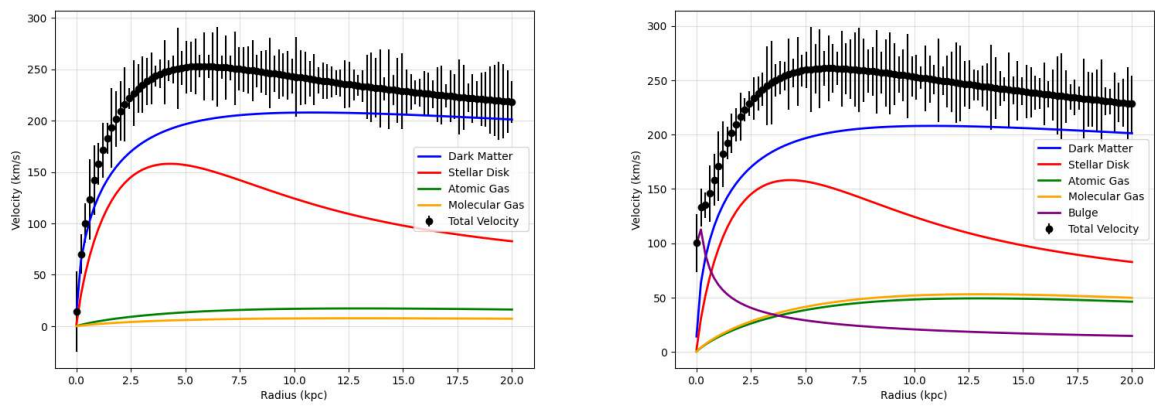
CHAPTER 3. TESTING GALAXY MOCK ROTATION CURVES



(a) MD1 : Burkert Halo DM model with no bulge component

(b) MD2 : Burkert Halo DM model with bulge

Figure 3.1: Burkert Halo Mock data. Black solid line with error bar represents our mock data for total velocity, which is then decomposed to dark matter (blue solid line) and baryonic components. Red, violet, green, and yellow represents stellar, bulge, atomic gas and molecular gas components.



(a) MD3 : NFW Halo DM model with no bulge component

(b) MD4 : NFW Halo DM model with bulge

Figure 3.2: NFW Halo Mock data. Black solid line with error bar represents our mock data for total velocity, which is then decomposed to dark matter (blue solid line) and baryonic components. Red, violet, green, and yellow represents stellar, bulge, atomic gas and molecular gas components.

This table 3.2 describes the MCMC fitting parameters and the equations used in the process. We have used $z = 0.3$ in our calculations. After fitting, we have corner and fitted plots as results for each case .

Burkert Halo	Input	NFW Halo	Input	Parameters	Details
Case 1	MD1	Case 5	MD3	r_0, ρ_0, R_d M_d, M_{HI}, M_{HII}	-
Case 2	MD1	Case 6	MD3	r_0, ρ_0, R_d, M_d	Values for M_{HI} and M_{HII} were predefined while modeling
Case 3	MD1	Case 7	MD3	r_0, ρ_0, R_d, M_d	M_{HI} and M_{HII} values were calculated using 2.6 and 2.5 using M_d
Case 4	MD2	Case 8	MD4	$r_0, \rho_0, R_d, M_d, M_b$	2.10 was used for bulge velocity calculation

Table 3.2: Comparison of Burkert and NFW Halo Models with Input Data and MCMC Parameters. Here, we have stellar disk mass (M_d), Stellar disk radius (R_d), Atomic gas mass (M_{HI}), Molecular gas mass (M_{H2}), Bulge mass (M_b), DM core/cusp radius (r_0) and DM core density (ρ_0)

3.1 Corner and fitted Plots

In this section we present corner plots and the best fitted rotation curves from MCMC fitting with mock data.

Corner plot (also known as a pair plot), is commonly used in Bayesian inference and MCMC (Markov Chain Monte Carlo) analyses to visualize the posterior distributions and parameter covariances of a model. The plot displays the joint and marginal posterior distributions of different parameters according to different cases ($r_0, \rho_0, R_d, M_d, M_{HI}, M_{H2}, M_b$). The **diagonal panels** show the **1D marginal posterior distributions** (histograms) of each individual parameter. The vertical blue line marks a true value. The **off-diagonal panels** show the **2D joint posterior distributions** between each pair of parameters. Black scatter plots and filled contours show how two parameters are correlated. Elliptical contours indicate the 1σ , 2σ , and 3σ confidence intervals. Blue cross-hairs mark true values in 2D. All the baryonic parameters are well constrained and in gaussian distribution. However, DM parameters r_0 and ρ_0 show non-Gaussian, skewed distributions, or even bimodal behavior.

As we know, a more circular covariance means that parameters are not correlated to each other, while elongated shapes indicate that the two parameters are correlated. Thus, we observe

that r_0 and ρ_0 are strongly correlated to each other pertaining to the elliptical contours. We also observe strong correlation of M_d with r_0 and ρ_0 , this strong correlation between the mass of the stellar disk (M_d) and the core density (ρ_0) and core radius (r_0) of the dark matter halo implies a degeneracy in how these components contribute to the overall mass distribution and dynamics of the galaxy—especially its rotation curve. This is a well-known problem in mass modeling of disk galaxies—often referred to as the **disk-halo degeneracy**. All the corner plots are [3.3a](#), [3.3c](#), [3.3e](#), [3.3g](#),[3.3i](#),[3.3k](#),[3.3m](#) and [3.3o](#).

Best fit rotation curve This plot presents a **galactic rotation curve decomposition** for the **mock galaxy**, using a **Burkert dark matter halo profile and NFW dark matter profile** and showing the contributions of various mass components to the observed rotational velocity ($V_{rot}(R)$ [km/s]) as a function of radius (R).

The solid thick blue line corresponds to the best-fit rotation curve derived from the fitted halo model. This line represents the total rotational velocity expected from the combined gravitational effects of dark matter, the stellar disk, gas components, and any central bulge. The black dashed line shows the contribution of the dark matter halo alone. This component becomes dominant at larger radii, reflecting the extended influence of dark matter in the galaxy's outskirts.

The yellow dashed line represents the contribution from the stellar disk, which typically dominates the inner region of the galaxy before declining with radius. The green dashed line indicates the effect of atomic hydrogen gas (HI), while the orange dashed line corresponds to the molecular gas (H_2). These gas components become increasingly important in the intermediate and outer regions of the galaxy. The brown dashed line represents the contribution of the bulge, which is significant primarily in the central few kiloparsecs. If no bulge is present, this component would be negligible or absent.

Observed rotation curve data are plotted as purple points with vertical error bars, representing measurement uncertainties. The alignment of these points with the blue best-fit curve indicates the quality of the model. Additionally, shaded blue regions surrounding the best-fit curve depict the 1σ , 2σ , and 3σ confidence intervals of the model, providing a visual sense of uncertainty in the rotational velocity prediction. All the best fitted plots are [3.3b](#),[3.3d](#),[3.3f](#),[3.3h](#),[3.3j](#),[3.3l](#)[3.3n](#) and [3.3p](#).

CHAPTER 3. TESTING GALAXY MOCK ROTATION CURVES

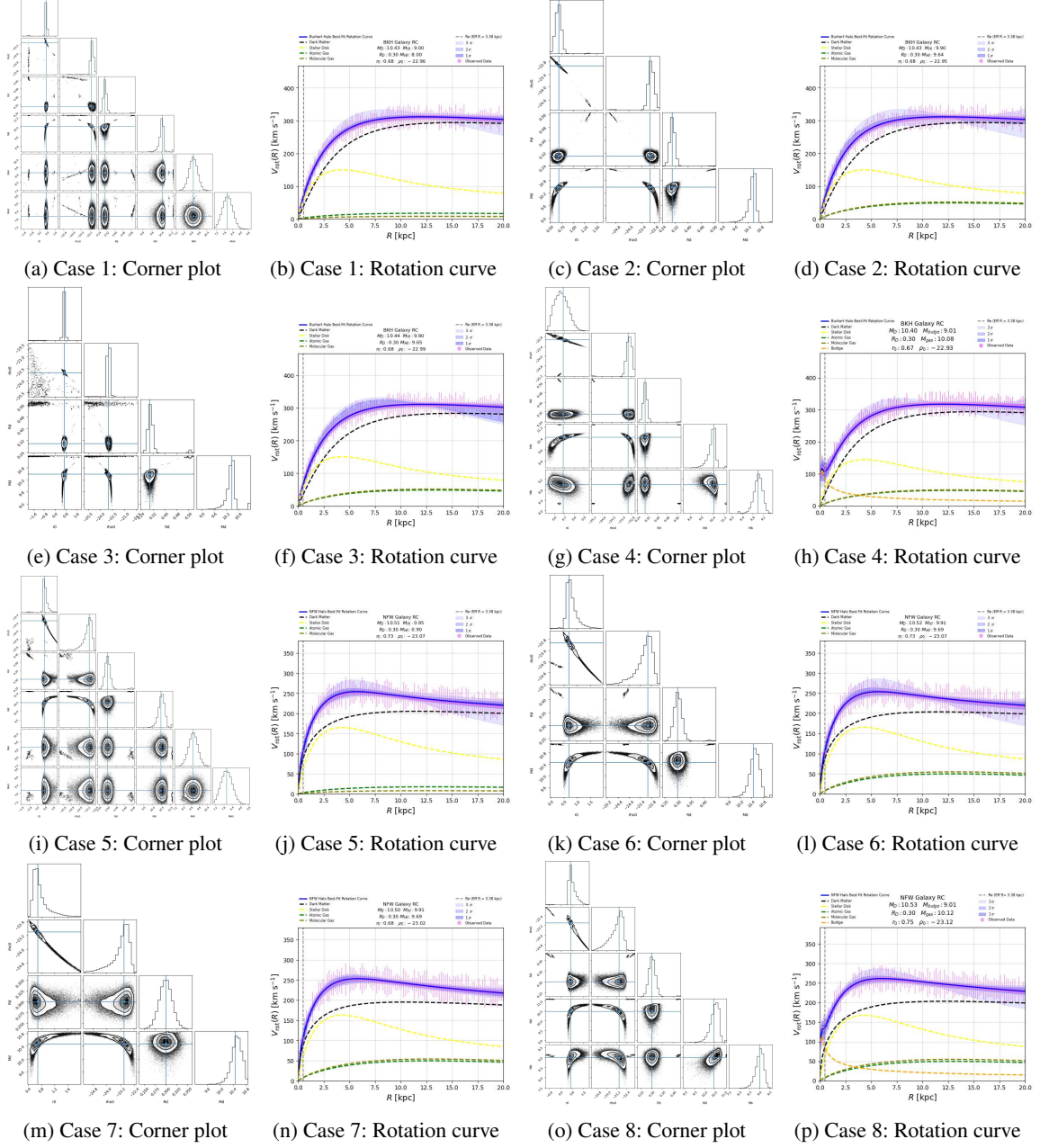


Figure 3.3: Summary of MCMC fitting results for all eight cases. Each row shows a corner plot (left) and the corresponding best-fit rotation curve (right). The corner plots illustrate the 1D and 2D posterior distributions of model parameters (r_0 , ρ_0 , R_d , M_d , M_{HI} , M_{HII} , M_b), highlighting correlations and uncertainties. The rotation curve plots decompose the contributions from different galaxy components (stellar disk, gas, bulge, and dark matter) and compare the model with mock observational data. Confidence intervals (1σ , 2σ , 3σ) are shaded around the total rotation curve. Blue cross-hairs mark true values in 2D. The thick blue line shows the best-fit total rotation curve from the halo model, combining contributions from all mass components. The black dashed line represents the dark matter halo, dominant at large radii. The yellow, brown, green, and orange dashed lines show the contributions from the stellar disk, bulge, atomic hydrogen (HI), and molecular gas (H_2), respectively.

3.2 Dark Matter Fraction

Using 2.18 equation, we can find the dark matter fraction of the 8 different cases as described in table 3.2.

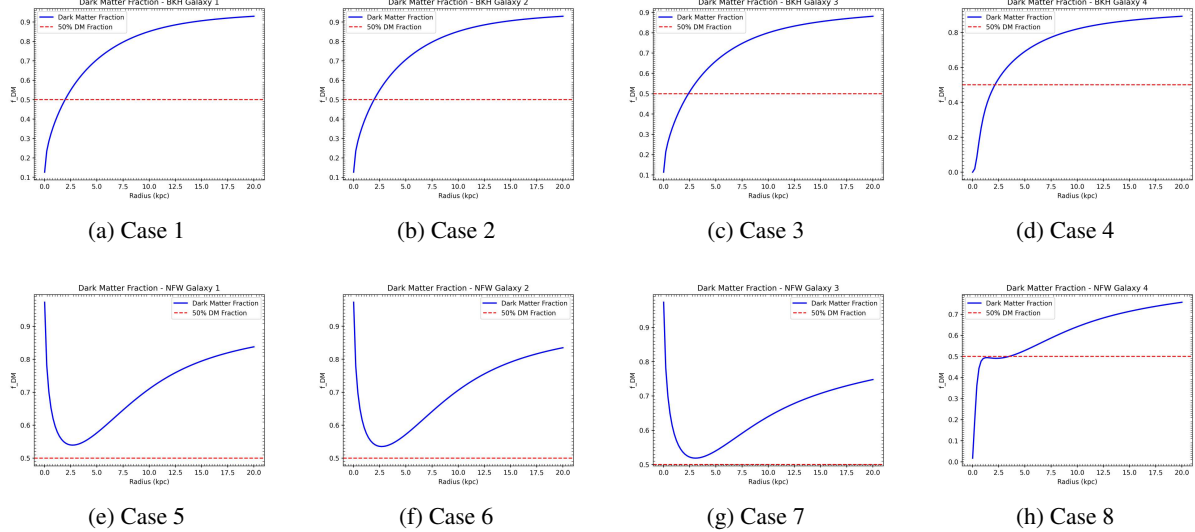


Figure 3.4: DM fraction (solid blue line) as a function of the radius in various velocity bins of mock galaxies. The red dashed line indicates the threshold at $f_{\text{DM}} = 0.5$, beyond which the galaxy is predominantly dark matter dominated. This trend is consistent with expectations from galaxy mass modeling, where baryonic matter dominates the inner regions and dark matter becomes increasingly significant at larger radii.

The dark matter (DM) fraction curves for the no-bulge case, shown in Figs. 3.4a–3.4c and 3.4e–3.4g, reflect the contrasting characteristics of the cored Burkert and cuspy NFW halo profiles. In the case of the Burkert halo, the DM fraction increases nearly linearly at small radii and transitions to a cubic growth at larger radii, consistent with its flat central density core. In contrast, the NFW halo displays a distinctive cuspy behavior: the DM fraction initially tends toward unity at very small radii, as the DM circular velocity closely matches the total velocity due to the $\rho \propto 1/r$ central divergence. This is followed by a decrease to a local minimum and a subsequent rise at larger radii. This trend highlights the inner dominance of dark matter in the NFW profile and its extended influence in the outskirts. Notably, in the no-bulge NFW case, the DM fraction remains above 50% at all radii, indicating that dark matter velocities dominate over baryonic contributions across the entire galactic disk.

Upon adding a bulge component, the qualitative features of the Burkert halo (Fig.3.4d) remain largely unchanged, reinforcing its cored nature, with a smooth and gradual transition to dark matter dominance. For the NFW halo with a bulge (Fig.3.4h), the effect of baryons becomes more apparent: the central regions show a reduced DM fraction, as the bulge significantly

contributes to the total mass. The DM fraction rises steeply again beyond a few kiloparsecs as the influence of the halo overtakes the baryonic mass. At intermediate radii, the curve may exhibit an inflection or mild plateau, marking the transition from baryon-dominated to dark matter-dominated regions. At large radii, in both models, the DM fraction asymptotically approaches unity as the baryonic contribution becomes negligible.

Overall, the DM fraction profiles underscore the fundamental differences between cored and cuspy halos: while the NFW model exhibits an early transition to dark matter dominance near the galactic center, the Burkert model shows a delayed and smoother transition, consistent with observations of low surface brightness and dwarf galaxies. These profiles also reflect the interplay between centrally concentrated baryonic matter and the extended dark matter halo, with the transition radius sensitively depending on the relative mass contributions of each component.

3.3 Analysis on multiple galaxies

To evaluate the robustness of our fitting algorithm across a range of galaxy types and parameter combinations, we adopt the parameter values from the previous analysis and systematically modify them, as summarized in Table 3.3.

$\log r_0$	$\log \rho_0$	$\log R_d$	$\log M_d$	$\log M_b$
0.69	-23	0.3	10.48	9
1	-23	0.3	10.48	9
0.84	-23	0.3	10.48	9
0.69	-22.5	0.3	10.48	9
0.69	-24	0.3	10.48	9
0.69	-23	0.48	10.48	9
0.69	-23	0.18	10.48	9
0.69	-23	0.3	11	9
0.69	-23	0.3	9.84	9
0.69	-23	0.3	10.48	10
0.69	-23	0.3	10.48	8

Table 3.3: Galaxy parameters for 11 mock galaxies with varying one parameters twice and keeping the others same. Here, we have stellar disk mass (M_d), Stellar disk radius (R_d), Bulge mass (M_b), DM core/cusp radius (r_0) and DM core density (ρ_0) in log units.

Using these parameter sets, we generated mock total velocity curves for 11 galaxies assuming a Burkert halo model and another 11 galaxies assuming an NFW halo model, resulting in a total of 22 mock galaxies. We then applied our fitting algorithm to this dataset, first using the Burkert halo fitting model and subsequently using the NFW halo fitting model. This procedure effectively produced 44 fitting cases in total.

For consistency, we maintained the same priors as those used in the earlier analysis. Representative examples of the resulting galaxy rotation curves, along with their corresponding corner plots, are presented below.

3.3.1 Burkert halo mock data and Burkert halo fitting

Each row shows a pair of plots per galaxy: the MCMC corner plot and the corresponding fitted rotation curve. The corner plots illustrate the 1D and 2D posterior distributions of model parameters ($r_0, \rho_0, R_d, M_d, M_{\text{HI}}, M_{\text{HII}}, M_b$), highlighting correlations and uncertainties. The rotation curve plots decompose the contributions from different galaxy components (stellar disk, gas, bulge, and dark matter) and compare the model with mock observational data. Confidence

CHAPTER 3. TESTING GALAXY MOCK ROTATION CURVES

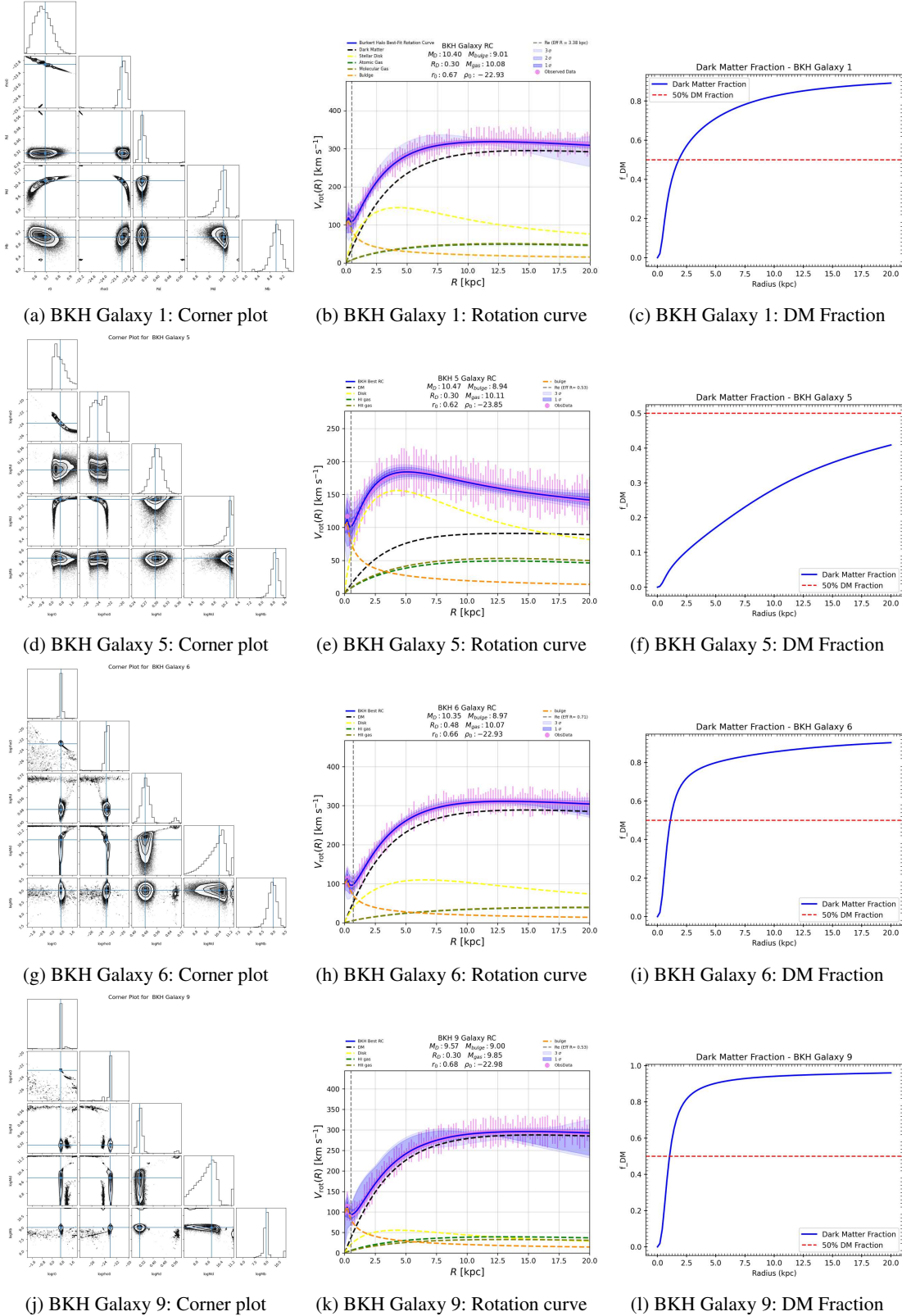


Figure 3.5: Corner Plots, Best fit rotation curves and DM fraction for Burkert mock galaxies 1,5,6 and 9

intervals (1σ , 2σ , 3σ) are shaded around the total rotation curve. Blue cross-hairs mark true values in 2D. The thick blue line shows the best-fit total rotation curve from the halo model, combining contributions from all mass components. The black dashed line represents the dark matter halo, dominant at large radii. The yellow, brown, green, and orange dashed lines show the contributions from the stellar disk, bulge, atomic hydrogen (HI), and molecular gas (H_2), respectively.

As shown in fig. 3.5, we have galaxy-wise analysis as:

Galaxy 1: Posterior is broader, especially in core radius or scale density, indicating a less tightly constrained fit. Yet the rotation curve fit appears visually acceptable. DM fraction follows the typical cored profiles behavior as described in section 3.2 for all galaxies.

Galaxy 5: Tight posteriors and a very good match between the model and mock data. Possibly the most reliable mock recovery among the four.

Galaxy 6: Similar to Galaxy 5 with good constraint and a well-behaved fit.

Galaxy 9: Shows moderate constraint but slightly broader posteriors than Galaxy 4 or 6. The fit is still good.

3.3.2 NFW halo mock data and Burkert halo fitting

Each row shows a pair of plots per galaxy: the MCMC corner plot and the corresponding fitted rotation curve. The corner plots illustrate the 1D and 2D posterior distributions of model parameters (r_0 , ρ_0 , R_d , M_d , M_{HI} , M_{HII} , M_b), highlighting correlations and uncertainties. The rotation curve plots decompose the contributions from different galaxy components (stellar disk, gas, bulge, and dark matter) and compare the model with mock observational data. Confidence intervals (1σ , 2σ , 3σ) are shaded around the total rotation curve. Blue cross-hairs mark true values in 2D. The thick blue line shows the best-fit total rotation curve from the halo model, combining contributions from all mass components. The black dashed line represents the dark matter halo, dominant at large radii. The yellow, brown, green, and orange dashed lines show the contributions from the stellar disk, bulge, atomic hydrogen (HI), and molecular gas (H_2), respectively. For NFW galaxy 7 and 10, we had to constrain our prior $0 < R_d < 2$ to get single contour regions.

As shown in fig. 3.6, all rotation curves show a reasonable match to the mock data, though

CHAPTER 3. TESTING GALAXY MOCK ROTATION CURVES

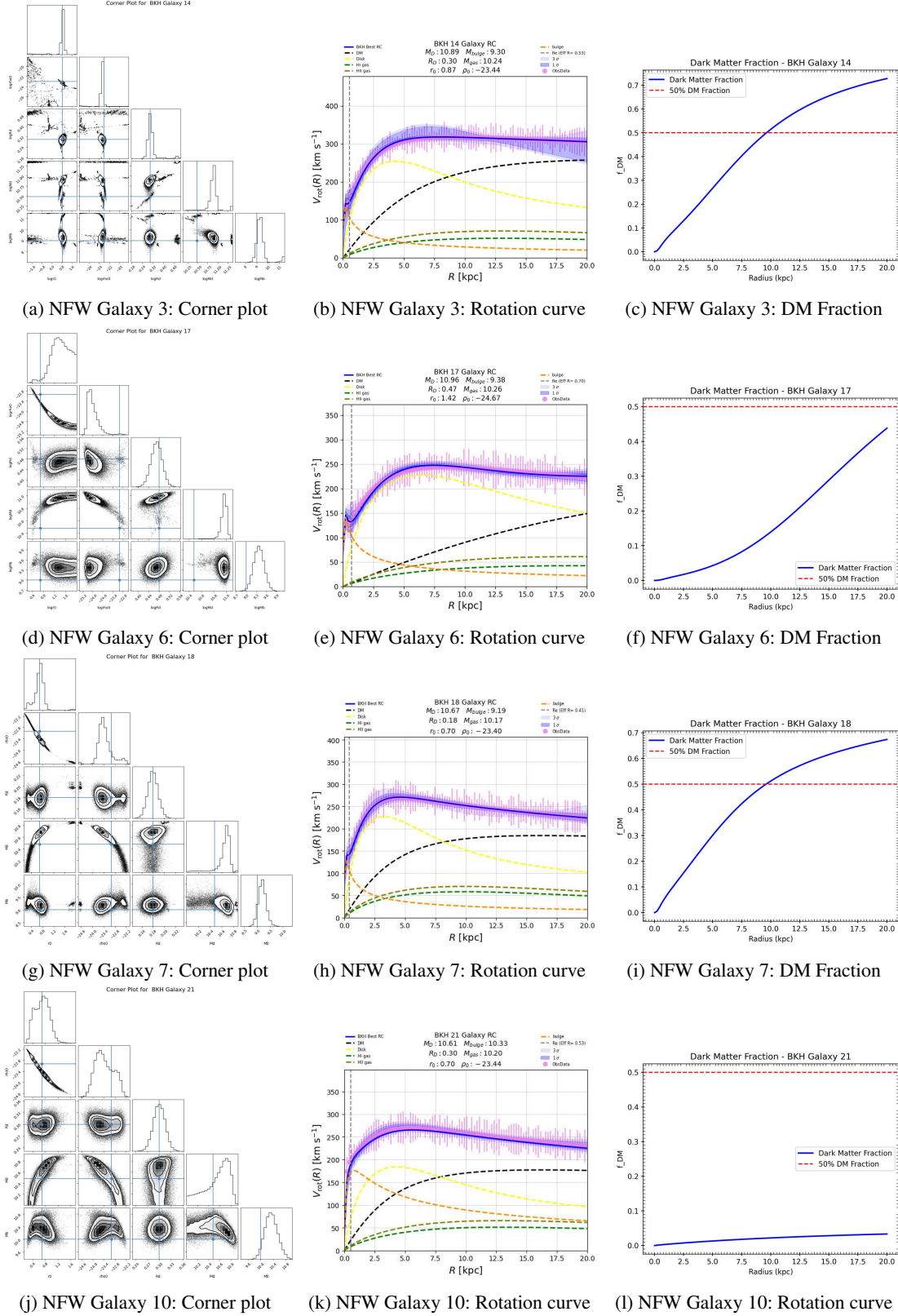


Figure 3.6: Corner plots and best-fit rotation curves for NFW mock galaxies 3, 6, 7, and 10.

some deviations may appear in the innermost regions. The slight discrepancies in inner fits may highlight the cored nature of Burkert failing to fit cuspy mock data well—an important point in dark matter modeling.

Galaxy 3: Shows broader posteriors than others, indicating higher uncertainty in parameter estimation, likely due to degenerate or noisy data. Some banana-shaped contours hint at parameter degeneracies.

Galaxy 5 and 10: Have tighter, well-constrained contours with clear maxima, indicating good parameter recovery.

Galaxy 7: Moderately constrained, with some correlation between parameters. Still acceptable.

For DM fraction curves, the Burkert fit underestimates the DM contribution in the inner regions and overestimates the baryonic dominance, leading to a systematic deviation from the true profile. This also highlights a fundamental limitation of cored halo models when applied to galaxies with intrinsically cuspy dark matter distributions

3.3.3 Burkert halo mock data and NFW halo fitting

Each row shows a pair of plots per galaxy: the MCMC corner plot and the corresponding fitted rotation curve. The corner plots illustrate the 1D and 2D posterior distributions of model parameters ($r_0, \rho_0, R_d, M_d, M_{\text{HI}}, M_{\text{HII}}, M_b$), highlighting correlations and uncertainties. The rotation curve plots decompose the contributions from different galaxy components (stellar disk, gas, bulge, and dark matter) and compare the model with mock observational data. Confidence intervals ($1\sigma, 2\sigma, 3\sigma$) are shaded around the total rotation curve. Blue cross-hairs mark true values in 2D. The thick blue line shows the best-fit total rotation curve from the halo model, combining contributions from all mass components. The black dashed line represents the dark matter halo, dominant at large radii. The yellow, brown, green, and orange dashed lines show the contributions from the stellar disk, bulge, atomic hydrogen (HI), and molecular gas (H_2), respectively.

As shown in fig. 3.7, Galaxy 1 & 5 : these have fairly tight posteriors, with visible degeneracies. NFW provides reasonable fits, but a slight overshoot is visible in the inner radii (cuspiness issue). This suggests that NFW compensates by tweaking parameters to approximate the cored

CHAPTER 3. TESTING GALAXY MOCK ROTATION CURVES

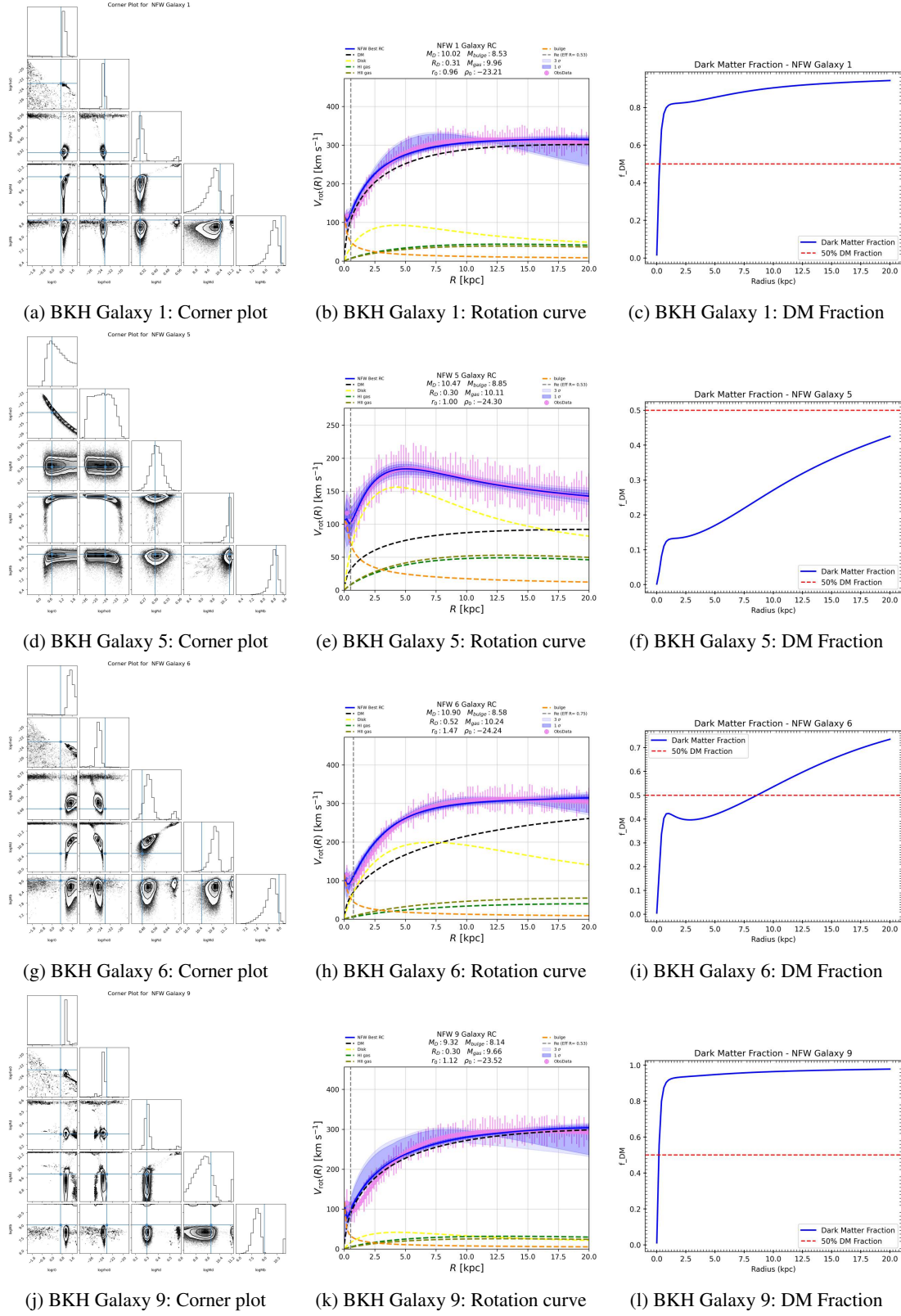


Figure 3.7: Corner plots and best-fit rotation curves for Burkert mock galaxies 1, 5, 6, and 9. .

shape.

Galaxy 6 : Broader, elongated posteriors, especially in ρ_s and r_s , showing significant degeneracy. This suggests NFW struggles to uniquely constrain these parameters when the true halo is cored (Burkert). Fit quality is visibly worse in the inner region. Reinforces that NFW cannot replicate a flat core.

Galaxy 9 : Similar to galaxy 6, inner region fit is not as good; model appears to over-predict the velocities.

For DM fraction curves, fitting a cuspy NFW profile to mock data from a cored Burkert halo results in a significant overestimation of the central dark matter fraction and an incorrectly early transition to DM dominance. The inferred mass profile does not accurately reflect the true core-like nature of the input, emphasizing the limitations of using cuspy models to fit galaxies with cored halo structures.

3.3.4 NFW halo mock data and NFW halo fitting

Each row shows a pair of plots per galaxy: the MCMC corner plot and the corresponding fitted rotation curve. The corner plots illustrate the 1D and 2D posterior distributions of model parameters ($r_0, \rho_0, R_d, M_d, M_{\text{HI}}, M_{\text{HII}}, M_b$), highlighting correlations and uncertainties. The rotation curve plots decompose the contributions from different galaxy components (stellar disk, gas, bulge, and dark matter) and compare the model with mock observational data. Confidence intervals ($1\sigma, 2\sigma, 3\sigma$) are shaded around the total rotation curve. Blue cross-hairs mark true values in 2D. The thick blue line shows the best-fit total rotation curve from the halo model, combining contributions from all mass components. The black dashed line represents the dark matter halo, dominant at large radii. The yellow, brown, green, and orange dashed lines show the contributions from the stellar disk, bulge, atomic hydrogen (HI), and molecular gas (H_2), respectively.

As shown in fig. 3.8,

For Galaxy 3 : the corner plot exhibits tightly clustered posterior distributions with minimal degeneracy among parameters, indicating robust constraints. The corresponding rotation curve fit aligns exceptionally well with the mock data across all radii, affirming the model's accuracy in parameter recovery under ideal conditions. DM fraction follows the typical cuspy behavior

CHAPTER 3. TESTING GALAXY MOCK ROTATION CURVES

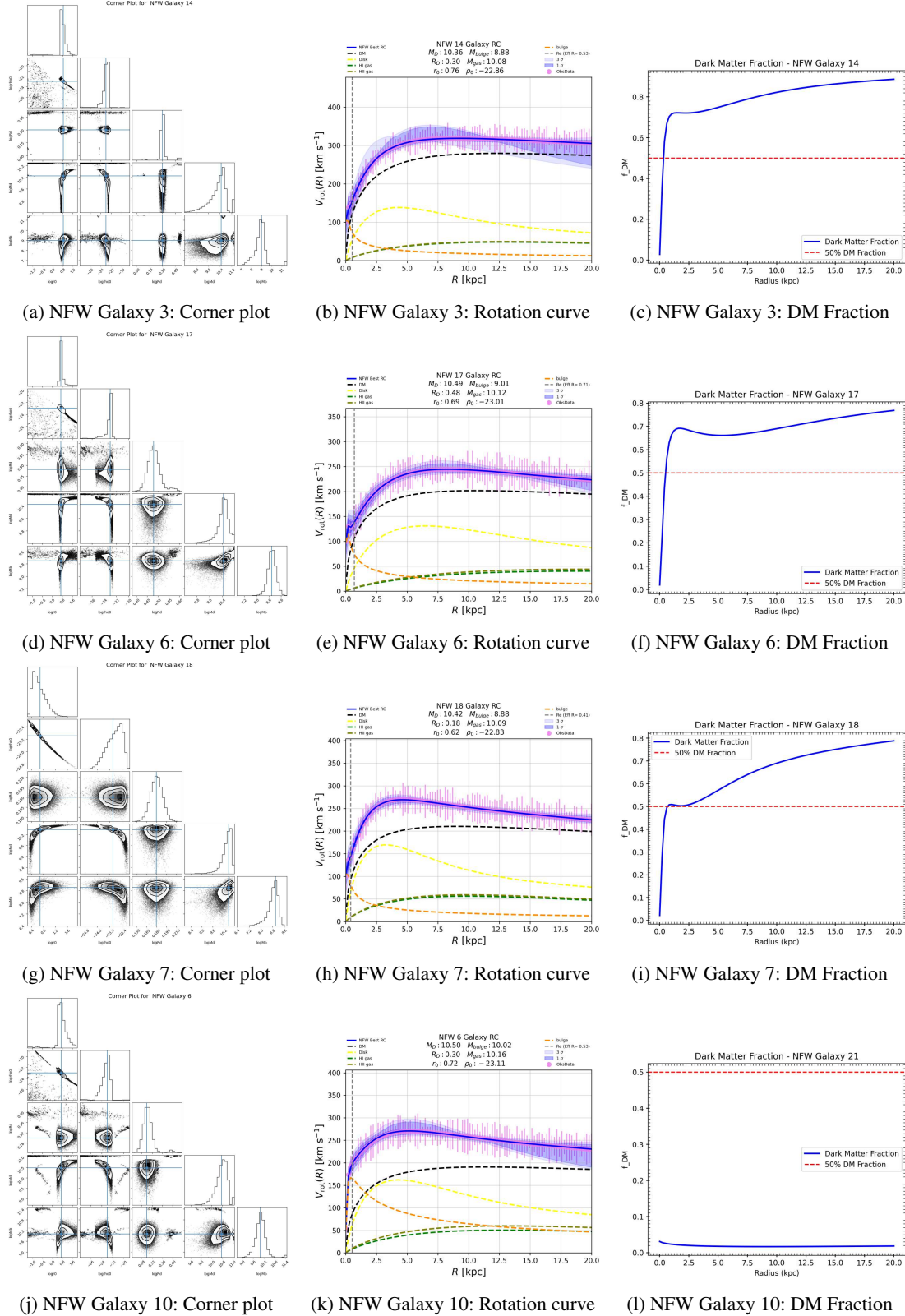


Figure 3.8: Corner plots and best-fit rotation curves for NFW mock galaxies 3, 6, 7, and 10.

as described in section 3.2, same for other galaxies.

In Galaxy 6 : the posterior distributions are similarly well-constrained, with sharp peaks and narrow contours. The rotation curve shows an excellent match with the input mock data, reinforcing the consistency of the NFW model when applied to self-generated datasets and further validating the MCMC fitting approach.

Galaxy 7 : it demonstrates slightly more complex behavior. While the corner plot reveals mild degeneracies—particularly between the scale radius and the halo concentration—the overall fit to the rotation curve remains highly accurate. This suggests that despite some parameter trade-offs, the model retains strong predictive capability and the recovered parameters are still meaningful.

For Galaxy 10 : the corner plot shows broader and more elongated contours, indicating stronger degeneracies in the parameter space. Nevertheless, the rotation curve reproduces the mock data closely. This implies that even in cases where parameters are not uniquely constrained, the NFW model can still provide a good description of the observed dynamics. DM fraction is pretty low indicating, for these set of parameters the baryons dominate the mass constituents of the galaxy.

3.3.5 Comparison with true values

In this section we present plots in which the modeled parameters are compared with true values for different galaxies. 3.9a shows NFW overestimates the values of r_0 in majority of the cases whereas for Burkert Halo model it is close to actual values except for some cases. 3.9b shows that ρ_0 values are in good agreement with true values for both the models. 3.10a , 3.10b and 3.11 show that predicted values are in good agreement with true values for both the models.

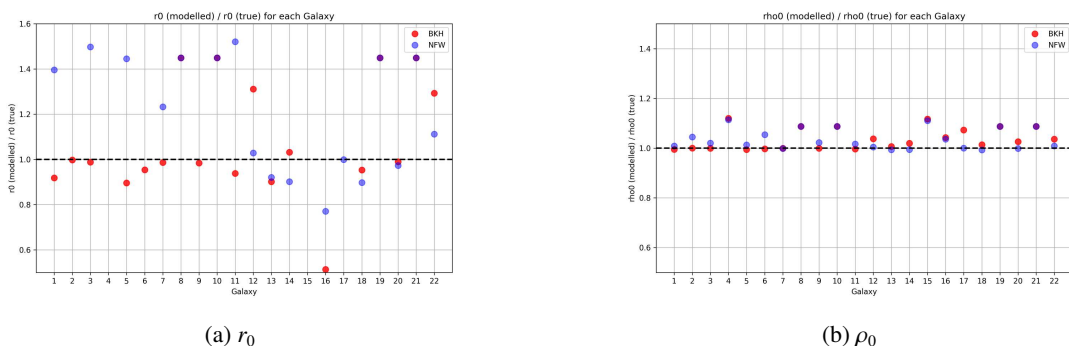


Figure 3.9: Dark matter parameters

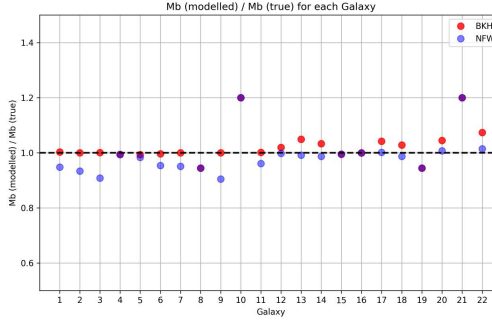


Figure 3.11: Bulge mass

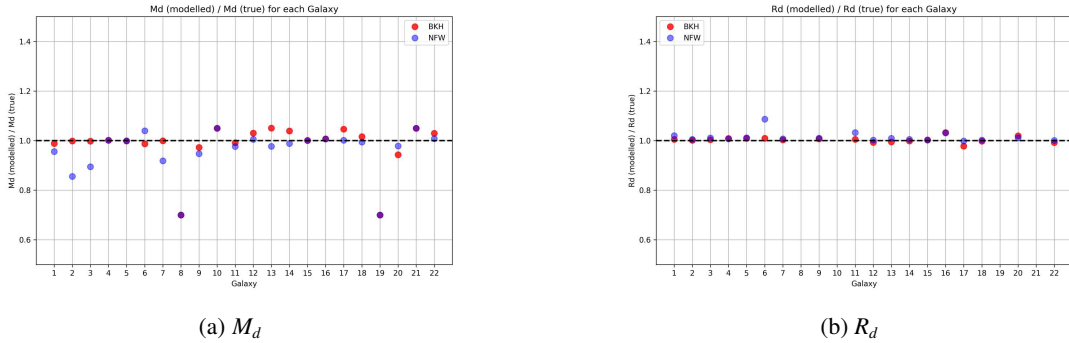


Figure 3.10: Baryonic parameters

3.3.6 Dark Matter Fraction

3.3.7 Inference

Upon analyzing the various combinations of mock data models and fitting models (figs. 3.5 – 3.8), we find that the fitting algorithm performs optimally when the mock data model and the fitting model are identical. However, when the mock and fitting models differ, notable discrepancies arise. Specifically, the Burkert halo fitting model tends to systematically overestimate the stellar disk mass when applied to mock data generated using the NFW halo model. Conversely, the NFW fitting model exhibits suboptimal performance when fitting mock data generated with a Burkert halo. The NFW profile performs well overall but struggles slightly with inner regions.

These trends are clearly illustrated in the comparison plots shown in figures 3.9, 3.10, and 3.11.

Chapter 4

MAGPI Observations

For this study, we use a sample of 303 galaxies from the *Middle Ages Galaxy Properties with Integral Field Spectroscopy* (MAGPI) survey. This is a major observational campaign aimed at studying the evolution of galaxies during a critical period in cosmic history—the so-called “cosmic noon,” roughly 3–4 billion years after the Big Bang (redshift $z \approx 0.3\text{--}0.4$) ([MAGPI Collaboration 2021](#)). This epoch is pivotal because it marks a time when the Universe was undergoing rapid transformation, with peak rates of star formation and active galactic nucleus (AGN) activity. MAGPI is an integral field spectroscopy (IFS) survey conducted using the *Multi Unit Spectroscopic Explorer* (MUSE) on the *Very Large Telescope* (VLT). It focuses on galaxies in the redshift range $z \approx 0.25\text{--}0.35$, bridging the gap between low-redshift (local universe) surveys like CALIFA and SAMI, and high-redshift studies such as those using KMOS or MOSFIRE (for details, see ([Foster et al. 2021](#))).

This [pdf](#) contains rotation curves from all the 303 galaxies with velocities and error bars. Along with this the plots contain the information on the redshift and emission line of the galaxies. We have marked Effective radius, optical radius and outer radius from the observations using yellow, red, blue dotted lines. The Point Spread Function (PSF) is shown by gray shaded area that characterizes how much the observed light distribution has been distorted by the instrument.

Bibliography

- Allen, Steven W., August E. Evrard, and Adam B. Mantz (Sept. 2011). “Cosmological Parameters from Observations of Galaxy Clusters”. In: 49.1, pp. 409–470. doi: [10.1146/annurev-astro-081710-102514](https://doi.org/10.1146/annurev-astro-081710-102514). arXiv: [1103.4829 \[astro-ph.CO\]](https://arxiv.org/abs/1103.4829).
- Babcock, Horace W. (Jan. 1939). In: *Lick Observatory Bulletin* 498, pp. 41–51. doi: [10.5479/ADS/bib/1939LicOB.19.41B](https://doi.org/10.5479/ADS/bib/1939LicOB.19.41B).
- Binney, James and Scott Tremaine (2008). *Galactic Dynamics: Second Edition*.
- Blok, W. J. G. de (Nov. 2009). “The Core-Cusp Problem”. In: *Advances in Astronomy* 2010.1. Ed. by Elias Brinks. ISSN: 1687-7977. doi: [10.1155/2010/789293](https://doi.org/10.1155/2010/789293). URL: <http://dx.doi.org/10.1155/2010/789293>.
- Bosma, A. (Dec. 1981). “21-cm line studies of spiral galaxies. II. The distribution and kinematics of neutral hydrogen in spiral galaxies of various morphological types.” In: 86, pp. 1825–1846. doi: [10.1086/113063](https://doi.org/10.1086/113063).
- Burkert, A. (July 1995). “The Structure of Dark Matter Halos in Dwarf Galaxies”. In: 447, pp. L25–L28. doi: [10.1086/309560](https://doi.org/10.1086/309560). arXiv: [astro-ph/9504041 \[astro-ph\]](https://arxiv.org/abs/astro-ph/9504041).
- Chowdhury, Aditya, Nissim Kanekar, and Jayaram N. Chengalur (2022). “Atomic Gas Scaling Relations of Star-forming Galaxies at $z \approx 1$ ”. In: *The Astrophysical Journal Letters* 941.1, p. L6. doi: [10.3847/2041-8213/ac9d8a](https://doi.org/10.3847/2041-8213/ac9d8a). URL: <https://doi.org/10.3847/2041-8213/ac9d8a>.
- de Blok, W. J. G., Stacy S. McGaugh, and Vera C. Rubin (Nov. 2001). “High-Resolution Rotation Curves of Low Surface Brightness Galaxies. II. Mass Models”. In: 122.5, pp. 2396–2427. doi: [10.1086/323450](https://doi.org/10.1086/323450).
- de Vaucouleurs, Gerard (Jan. 1948). “Recherches sur les Nebuleuses Extragalactiques”. In: *Annales d’Astrophysique* 11, p. 247.
- Donato, Fiorenza, Gianfranco Gentile, and Paolo Salucci (Sept. 2004). “Cores of dark matter haloes correlate with stellar scalelengths”. In: *Monthly Notices of the Royal Astronomical Society* 353.2, pp. L17–L22. ISSN: 0035-8711. doi: [10.1111/j.1365-2966.2004.08220](https://doi.org/10.1111/j.1365-2966.2004.08220).

- x. eprint: <https://academic.oup.com/mnras/article-pdf/353/2/L17/3878121/353-2-L17.pdf>. URL: <https://doi.org/10.1111/j.1365-2966.2004.08220.x>.
- European Space Agency (Oct. 2019). *Cosmic Energy Budget*. Accessed: 2025-05-06. URL: <https://sci.esa.int/s/ABdZM5W>.
- Foreman-Mackey, Daniel, David W. Hogg, Dustin Lang, and Jonathan Goodman (Mar. 2013). “emcee: The MCMC Hammer”. In: 125.925, p. 306. doi: [10.1086/670067](https://doi.org/10.1086/670067). arXiv: [1202.3665 \[astro-ph.IM\]](https://arxiv.org/abs/1202.3665).
- Foster, C. et al. (2021). “The MAGPI survey: Science goals, design, observing strategy, early results and theoretical framework”. In: *Publications of the Astronomical Society of Australia* 38. ISSN: 1448-6083. doi: [10.1017/pasa.2021.25](https://doi.org/10.1017/pasa.2021.25). URL: <http://dx.doi.org/10.1017/pasa.2021.25>.
- Freeman, K. C. (June 1970). “On the Disks of Spiral and S0 Galaxies”. In: 160, p. 811. doi: [10.1086/150474](https://doi.org/10.1086/150474).
- Hernquist, Lars (June 1990). “An Analytical Model for Spherical Galaxies and Bulges”. In: 356, p. 359. doi: [10.1086/168845](https://doi.org/10.1086/168845).
- Hon, Dexter S -H, Alister W Graham, and Nandini Sahu (Dec. 2022). “The size–mass and other structural parameter (n, z, Rz) relations for local bulges/spheroids from multicomponent decompositions”. In: *Monthly Notices of the Royal Astronomical Society* 519.3, pp. 4651–4669. ISSN: 0035-8711. doi: [10.1093/mnras/stac3704](https://doi.org/10.1093/mnras/stac3704). eprint: <https://academic.oup.com/mnras/article-pdf/519/3/4651/48745006/stac3704.pdf>. URL: <https://doi.org/10.1093/mnras/stac3704>.
- Jeans, J. H. (Jan. 1922). “The Motions of Stars in a Kapteyn-Universe”. In: *Monthly Notices of the Royal Astronomical Society* 82.3, pp. 122–132. ISSN: 0035-8711. eprint: <https://academic.oup.com/mnras/article-pdf/82/3/122/18250702/mnras82-0122.pdf>. URL: <https://doi.org/10.1093/mnras/82.3.122>.
- Kapteyn, J. C. (May 1922). “First Attempt at a Theory of the Arrangement and Motion of the Sidereal System”. In: 55, p. 302. doi: [10.1086/142670](https://doi.org/10.1086/142670).
- Karukes, E. V. and P. Salucci (Nov. 2016). “The universal rotation curve of dwarf disc galaxies”. In: *Monthly Notices of the Royal Astronomical Society* 465.4, pp. 4703–4722. ISSN: 1365-2966. doi: [10.1093/mnras/stw3055](https://doi.org/10.1093/mnras/stw3055). URL: <http://dx.doi.org/10.1093/mnras/stw3055>.
- Knudsen, Ole (2005). “Chapter 58 - Lord Kelvin, Baltimore lectures on mathematical physics ((1884), 1904)”. In: *Landmark Writings in Western Mathematics 1640-1940*. Ed. by I. Grattan-Guinness, Roger Cooke, Leo Corry, Pierre Crépel, and Niccolo Guicciardini. Amsterdam: Elsevier Science, pp. 748–756. ISBN: 978-0-444-50871-3. doi: <https://doi.org/10.1093/acprof:oso/9780444508713.003.0058>.

- [org/10.1016/B978-044450871-3/50139-X](https://doi.org/10.1016/B978-044450871-3/50139-X). URL: <https://www.sciencedirect.com/science/article/pii/B978044450871350139X>.
- Lagos, Claudia del P., Carlton M. Baugh, Cedric G. Lacey, Andrew J. Benson, Han-Seek Kim, and Chris Power (Dec. 2011). “Cosmic evolution of the atomic and molecular gas contents of galaxies”. In: *Monthly Notices of the Royal Astronomical Society* 418.3, pp. 1649–1667. ISSN: 0035-8711. doi: [10.1111/j.1365-2966.2011.19583.x](https://doi.org/10.1111/j.1365-2966.2011.19583.x). eprint: <https://academic.oup.com/mnras/article-pdf/418/3/1649/18438678/mnras0418-1649.pdf>. URL: <https://doi.org/10.1111/j.1365-2966.2011.19583.x>.
- MAGPI Collaboration (2021). *MAGPI Survey: Middle Ages Galaxy Properties with Integral field spectroscopy*. <https://magpisurvey.org/index.html>. Accessed: 2025-05-09.
- Navarro, Julio F., Carlos S. Frenk, and Simon D. M. White (May 1996). “The Structure of Cold Dark Matter Halos”. In: 462, p. 563. doi: [10.1086/177173](https://doi.org/10.1086/177173). arXiv: [astro-ph/9508025 \[astro-ph\]](https://arxiv.org/abs/astro-ph/9508025).
- Oort, J. H. (Aug. 1932). “The force exerted by the stellar system in the direction perpendicular to the galactic plane and some related problems”. In: 6, p. 249.
- Öpik, E. (2022). *The question of selective absorption of light in space viewed from the viewpoint of the dynamics of the universe*. arXiv: [2203.14871 \[astro-ph.GA\]](https://arxiv.org/abs/2203.14871). URL: <https://arxiv.org/abs/2203.14871>.
- Palunas, Povilas and T. B. Williams (Dec. 2000). “Maximum Disk Mass Models for Spiral Galaxies”. In: 120.6, pp. 2884–2903. doi: [10.1086/316878](https://doi.org/10.1086/316878). arXiv: [astro-ph/0009161 \[astro-ph\]](https://arxiv.org/abs/astro-ph/0009161).
- Paolo, C. Di, P. Salucci, and A. Erkurt (2019). “The Universal Rotation Curve of Spiral Galaxies – IV. The Dark Matter Distribution out to the Virial Radius”. In: *Monthly Notices of the Royal Astronomical Society* 490.4, pp. 5451–5468. doi: [10.1093/mnras/stz2840](https://doi.org/10.1093/mnras/stz2840). URL: <https://doi.org/10.1093/mnras/stz2840>.
- Peebles, P. J. E. (1993). *Principles of Physical Cosmology*. Princeton University Press. doi: [10.1515/9780691206721](https://doi.org/10.1515/9780691206721).
- Persic, Massimo, Paolo Salucci, and Fulvio Stel (July 1996). “The universal rotation curve of spiral galaxies — I. The dark matter connection”. In: 281.1, pp. 27–47. doi: [10.1093/mnras/278.1.27](https://doi.org/10.1093/mnras/278.1.27). arXiv: [astro-ph/9506004 \[astro-ph\]](https://arxiv.org/abs/astro-ph/9506004).
- Poincaré, H. and H. Vergne (1911). *Leçons sur les hypothèses cosmogoniques professées à la Sorbonne par Henri Poincaré*. Cours de la Faculté des sciences de Paris. A. Hermann. URL: <https://books.google.co.in/books?id=itMT0QEACAAJ>.

- Rubin, V. C., W. K. Ford Jr., and N. Thonnard (Nov. 1978). “Extended rotation curves of high-luminosity spiral galaxies. IV. Systematic dynamical properties, Sa -*i* Sc.” In: 225, pp. L107–L111. doi: [10.1086/182804](https://doi.org/10.1086/182804).
- Rubin, Vera C. and W. Kent Ford Jr. (Feb. 1970). “Rotation of the Andromeda Nebula from a Spectroscopic Survey of Emission Regions”. In: 159, p. 379. doi: [10.1086/150317](https://doi.org/10.1086/150317).
- Salucci, P. and A. Burkert (July 2000). “Dark Matter Scaling Relations”. In: *The Astrophysical Journal* 537.1, pp. L9–L12. ISSN: 0004-637X. doi: [10.1086/312747](https://doi.org/10.1086/312747). URL: <http://dx.doi.org/10.1086/312747>.
- Salucci, P., A. Lapi, C. Tonini, G. Gentile, I. Yegorova, and U. Klein (June 2007). “The universal rotation curve of spiral galaxies - II. The dark matter distribution out to the virial radius”. In: *Monthly Notices of the Royal Astronomical Society* 378.1, pp. 41–47. ISSN: 1365-2966. doi: [10.1111/j.1365-2966.2007.11696.x](https://doi.org/10.1111/j.1365-2966.2007.11696.x). URL: <http://dx.doi.org/10.1111/j.1365-2966.2007.11696.x>.
- Salucci, Paolo (Feb. 2019). “The distribution of dark matter in galaxies”. In: *The Astronomy and Astrophysics Review* 27.1. ISSN: 1432-0754. doi: [10.1007/s00159-018-0113-1](https://doi.org/10.1007/s00159-018-0113-1). URL: <http://dx.doi.org/10.1007/s00159-018-0113-1>.
- Sharma, Gauri (2021). “Nature of Dark Matter from Astrophysics of High Redshift Star-forming Galaxies”. PhD thesis. SISSA - Via Bonomea 265 – 34136 Trieste - Italy: Scuola Internazionale Superiore di Studi Avanzati, Trieste, Italy.
- Sharma, Gauri, Paolo Salucci, and Glenn van de Ven (Mar. 2022). “Observational evidence of evolving dark matter profiles at z1”. In: *Astronomy and Astrophysics* 659, A40. ISSN: 1432-0746. doi: [10.1051/0004-6361/202141822](https://doi.org/10.1051/0004-6361/202141822). URL: <http://dx.doi.org/10.1051/0004-6361/202141822>.
- Simon, Joshua D., Alberto D. Bolatto, Adam Leroy, Leo Blitz, and Elinor L. Gates (Mar. 2005). “High-Resolution Measurements of the Halos of Four Dark Matter-Dominated Galaxies: Deviations from a Universal Density Profile*”. In: *The Astrophysical Journal* 621.2, p. 757. doi: [10.1086/427684](https://doi.org/10.1086/427684). URL: <https://doi.org/10.1086/427684>.
- Smith, Sinclair (Jan. 1936). “The Mass of the Virgo Cluster”. In: 83, p. 23. doi: [10.1086/143697](https://doi.org/10.1086/143697).
- Speagle, J. S., C. L. Steinhardt, P. L. Capak, and J. D. Silverman (Oct. 2014). “A Highly Consistent Framework for the Evolution of the Star-Forming “Main Sequence” from z ~0-6”. In: 214.2, 15, p. 15. doi: [10.1088/0067-0049/214/2/15](https://doi.org/10.1088/0067-0049/214/2/15). arXiv: [1405.2041](https://arxiv.org/abs/1405.2041) [[astro-ph.GA](#)].
- Tacconi, L. J. et al. (Feb. 2018). “PHIBSS: Unified Scaling Relations of Gas Depletion Time and Molecular Gas Fractions*”. In: *The Astrophysical Journal* 853.2, p. 179. ISSN: 1538-

BIBLIOGRAPHY

4357. doi: [10.3847/1538-4357/aaa4b4](https://doi.org/10.3847/1538-4357/aaa4b4). URL: <http://dx.doi.org/10.3847/1538-4357/aaa4b4>.

Zwicky, F. (Jan. 2009). “Republication of: The redshift of extragalactic nebulae”. In: *General Relativity and Gravitation* 41.1, pp. 207–224. doi: [10.1007/s10714-008-0707-4](https://doi.org/10.1007/s10714-008-0707-4).